Originals

Experiments in Fluids 18 (1994) 1–9 © Springer-Verlag 1994

Azimuthal velocity in supercritical circular Couette flow

S. T. Wereley, R. M. Lueptow

Abstract Although the stability of supercritical circular Couette flow has been studied extensively, results for the velocity field of the flow are limited. The azimuthal velocity profiles for the Taylor vortex, wavy vortex, and turbulent Taylor vortex flow in the annulus between a rotating inner cylinder and a fixed outer cylinder with fixed end conditions were measured using laser Doppler velocimetry. The azimuthal velocity was measured at about 300 points per vortex pair, distributed in both the radial and axial directions. This measurement procedure was repeated for several Reynolds numbers within each flow regime to study both the spatial dependence and the Reynolds number dependence of the azimuthal velocity. The experimental results for the Taylor vortex flow regime compare well with the Davey perturbation expansion of the Navier-Stokes equations about the circular Couette flow solution [J. Fluid Mech. 14, 336 (1962)]. The measured azimuthal velocity fields also indicate two predominant effects with increasing Reynolds number: the magnitude of the radial gradient of azimuthal velocity near both cylinders increases and the radial outflow region between pairs of vortices becomes increasingly jet-like.

1 Introduction

Supercritical circular Couette flow between concentric rotating cylinders has been studied for over a century since Mallock (1888) first attempted to measure the viscosity of water experimentally. Since then all manner of experimental, numerical, and theoretical analyses of the flow have been undertaken, with most directed toward the stability of the flow. Few researchers have studied the velocity profiles that develop in the annulus between concentric cylinders, the inner one rotating and the outer one fixed, even though an understanding of the velocity field is crucial to engineering applications of the flow such as rotating filter separators used for separation of blood, oily emulsions, and particulate from combustion gases.

Received: 23 September 1993/Accepted: 23 May 1994

S. T. Wereley, R. M. Lueptow
Department of Mechanical Engineering, Northwestern University, Evanston, IL 60208, USA

Correspondence to: R.M. Lueptow

This work was supported by Baxter Healthcare Corporation and The Whitaker Foundation

The measurements of the velocity field for supercritical circular Couette flow described in this paper were focused toward two objectives. The first objective was to determine the extent of the validity of Davey's (1962) analytical prediction of the velocity field for Taylor vortex flow by measuring the azimuthal velocity field over the radial and axial extent of a vortex pair for several Reynolds numbers. The second objective was to examine the development of the azimuthal velocity field with Reynolds number in the Taylor vortex, wavy vortex, modulated wavy vortex, and turbulent vortex flow regimes.

Several limited measurements of the velocity field of Taylor vortex flow have been made in an attempt to experimentally confirm Davey's (1962) perturbation expansion of the Navier-Stokes equations about the circular Couette flow solution. Heinrichs, et al. (1988) used laser Doppler velocimetry (LDV) to measure the axial velocity in Taylor vortex flow at a series of points distributed in the axial direction for a fixed radial position. They confirmed that the Fourier coefficients of the axial velocity grow as Davey predicted. Gollub and Freilich (1976) and Berland, et al. (1986) made similar measurements of the radial velocity at a fixed radial position and several axial positions using LDV. Both groups also found that the Fourier coefficients of the radial velocity grow as Davey predicted.

While the validity of a single aspect of Davey's perturbation expansion for Taylor vortex flow has been confirmed as described above, the focus has been on the growth rate of the Fourier coefficients of a single component of the velocity field. Although this is a crucial part of the Davey expansion, other issues have not been addressed. First, although the growth rates of the Fourier coefficients have been examined, the magnitude of the velocity fields they produce has not. Second, the radial dependence of Davey's expansion has not been confirmed by experiment. Finally, the velocity field derived from Davey's expansion has not been compared to an experimentally measured velocity field.

In this paper, we explore the unresolved issues related to Davey's expansion for the velocity field in Taylor vortex flow. Toward that end, we calculated the Davey expansion for the radius ratio of the experimental apparatus used in this study. Then we measured both the radial and axial dependence of the azimuthal velocity field spanning a full vortex pair as a function of Reynolds number for the configuration with the inner cylinder rotating and the outer cylinder fixed, comparing the experimentally measured velocity field for Taylor vortex flow directly to the velocity field predicted by Davey's expansion.

Although there have been several numerical simulations of wavy vortex flow (Coughlin and Marcus, 1992; Marcus, 1984;

Moser et al., 1983), only a few experimental measurements of the velocity field for higher order supercritical circular Couette flow regimes have been made. Taylor (1936) measured the azimuthal velocity profile in turbulent Taylor vortex flow using a Pitot tube and found that the angular momentum of the azimuthal flow was independent of radial position for a large portion of the annular gap. Steep velocity gradients appeared near the inner and outer walls. Smith and Townsend (1982) used hot wire anemometry to measure the radial and axial dependence of the azimuthal velocity profile for turbulent Taylor vortex flow. They superimposed a small axial flow on the turbulent Taylor vortex flow in order to slowly sweep the Taylor cells past the hot wire probe. Knowing the axial flow rate, they were able to reconstruct the axial dependence of the azimuthal velocity. Gollub and Swinney (1975) made extensive measurements of the radial velocity at a single location in the annulus for a large range of Reynolds numbers using LDV. By comparing the power spectra associated with the velocity signals from the different flow regimes, they were able to demonstrate that the Landau picture of the transition to turbulence is not accurate.

The few measurements of the velocity field for supercritical circular Couette flow made by previous researchers have been very limited in scope, typically only a small number of spatial locations. Here we consider both the radial and axial dependence of the velocity field spanning a full vortex pair as a function of Reynolds number for the configuration with the inner cylinder rotating and the outer cylinder fixed. We present laser Doppler velocimetry measurements of the azimuthal velocity as a function of radial and axial position as well as Reynolds number for all of the major flow regimes encountered in the Taylor vortex flow system: Taylor vortex flow, wavy vortex flow, and turbulent Taylor vortex flow. These velocity measurements are used to examine the change in the strength of the vortices with Reynolds number, the effect of the secondary vortex flow on the distribution of the azimuthal velocity, and the change in the gradient of the velocity near the walls of the annulus with Reynolds number. Further, the results for wavy vortex flow are compared to the numerical computations of Marcus (1984).

2 Davey's expansion for Taylor vortex flow

The radius ratio and the Reynolds number are important dimensionless parameters governing the flow between concentric cylinders with the inner cylinder rotating and the outer cylinder fixed. The radius ratio is defined as $\eta = r_i/r_0$, where r_i is the radius of the inner cylinder and r_0 is the radius of the outer cylinder. These are several common means of non-dimensionalizing the inner cylinder speed. In this paper we use the rotating Reynolds number defined as $Re = r_i \Omega d/\nu$, where Ω is the angular speed of the inner cylinder, $d = r_0 - r_i$ is the gap between the inner cylinder and the outer cylinder, and ν is the kinematic viscosity. When the Reynolds number exceeds a particular critical value, denoted Re_C, counter-rotating pairs of toroidal vortices appear in the annulus as a result of a centrifugal instability. The critical Reynolds number Re_C is strongly dependent upon the radius ratio η.

Taylor (1923) was the first to perform a linear stability analysis of the concentric cylinder system against axisymmetric perturbations assuming that the annular gap was small compared to the radii of the cylinders so that η approaches 1. His calculated value of Re_C matched to within 2% the value he obtained experimentally. Chandrasekhar (1958) reformulated Taylor's work and extended it to the finite gap size case, $0 < \eta < 1$. Stuart (1960) and Watson (1960) showed that the growth of infinitesimal disturbances in the circular Couette flow regime is governed by a form of the nonlinear Landau equation.

Davey combined the work of Chandrasekhar, Stuart, and Watson to develop a perturbation expansion for the full field velocity profile accurate near the transition from circular Couette flow to Taylor vortex flow. He began by expanding the disturbance portion of each velocity component in a Fourier series. The azimuthal velocity was expanded as

$$v_\theta(r, z, t, \varepsilon) = \bar{v}_\theta(r, t, \varepsilon) + \sum_{n=1}^{\infty} v_n(r, t, \varepsilon) \cos n\lambda z \tag{1}$$

where r is the radial position, z is the axial position, t is time, v_θ is the instantaneous azimuthal velocity at a particular position, $\bar{v}_\theta$ is the axially averaged velocity, v_n is the nth Fourier coefficient, $\varepsilon = 1 - (Re_C/Re)^2$ is the reduced Reynolds number, and λ is the fundamental wavenumber in the axial direction. The remaining velocity components and the pressure were expanded similarly. Following Stuart and Watson, Davey expanded the Fourier coefficients of the velocity components in a power series. The azimuthal component was expanded as

$$v_n(r, t, \varepsilon) = \sum_{m=0}^{\infty} A(t, \varepsilon)^{n+2m} v_{nm}(r), \tag{2}$$

where A is the generalized amplitude coefficient, and v_{nm} are the power series coefficients that carry the radial dependence. The presence of the vortices disturbs the azimuthal velocity from its circular Couette flow value according to

$$\bar{v}_\theta(r, t, \varepsilon) = \bar{v}_c(r) + \sum_{m=1}^{\infty} A(t, \varepsilon)^{2m} f_m(r) \tag{3}$$

where $\bar{v}_c$ is the stable circular Couette flow profile and the f_m are power series coefficients that carry the radial dependence.

The generalized amplitude coefficient satisfies the time dependent Landau equation

$$\frac{\partial A(t, \varepsilon)}{\partial t} = \sum_{m=0}^{\infty} a_m A(t, \varepsilon)^{2m+1} \tag{4}$$

Davey found that the generalized amplitude coefficient for the time independent case, called the equilibrium amplitude $A_e(\varepsilon)$, was adequately approximated by only the first two terms of Eq. (4), leaving

$$A_e(\varepsilon) = \sqrt{-a_0(\varepsilon)/a_1} = \sqrt{-\sigma(\varepsilon)/a_1} \tag{5}$$

where a_0 is defined to be equal to σ, the growth parameter. Davey showed that σ is proportional to ε, leading to the relation that

$$A_e(\varepsilon) = k Re_C \sqrt{\varepsilon} \tag{6}$$

where k is some constant that remains to be determined.

Davey substituted the above expressions into the full Navier-Stokes equations and simplified the result using the required independence of the solution with respect to rotation about the

cylinders' common axis and its independence of time. Collecting terms with like powers of A_e, he arrived at a system of linear differential equations numerically solvable for the power series coefficients v_{nm} and f_m, the critical Reynolds number Re_C, the axial wavenumber at transition λ_c, and the unknown constant k.

Davey used the results of his perturbation expansion to calculate the torque required to keep the inner cylinder spinning at a constant rate when Taylor vortices are present. He generated numerical results for a wide gap case, $\eta = 0.5$, and the narrow gap limit, η approaching 1. He compared these results to torque experiments performed by Taylor (1923) and Donnelly and Simon (1960). Davey found that for $\varepsilon \ll 1$, the range of validity of his expansion, his narrow gap results agreed quite well with experiment. For the wide gap case, his results agreed with experimental results over an even larger range.

Several subsequent researchers have also compared portions of Davey's work with experiment. Snyder and Lambert (1966) used a thermistor-based shear probe to measure the shear at the surface of the outer cylinder for the wide gap case of $\eta = 0.5$. They found that their data, which had 8% uncertainty, agreed with Davey's expansion for $\varepsilon \leqslant 0.75$. They also found the first four normal modes present in the disturbed velocity field to be in phase with each other, confirming one of Davey's primary assumptions. Heinrichs, et al. (1988), Gollub and Freilich (1976), and Berland, et al. (1986) all used LDV to measure a single velocity component of the disturbed flow at a single radial position and several axial locations. Although all three experiments were performed for different radius ratios than Davey used in his calculations, $\eta = 0.612$, 0.598, and 0.747, respectively, they all affirmed that based on the Fourier components A_e should be proportional to $\sqrt{\varepsilon}$ for $\varepsilon \leqslant 1$, by showing that the coefficients of the Fourier components of the disturbed velocity field grow as Davey predicted. Nevertheless, they did not specifically address the growth of A_e with ε, the radial validity of Davey's expansion, or the validity of the velocity field derived from Davey's expansion, all of which are addressed here.

3
Experimental setup

The flow cell used for the experiments described here is shown in Fig. 1. It consisted of a pair of concentric acrylic cylinders, the inner one rotating and the outer one fixed. The flow cell was made of clear acrylic to allow both optical access to the flow for the LDV and to permit excess laser light to exit the flow cell, minimizing both heating effects from laser light absorption and background noise from spurious laser light reflections. The radius ratio of the flow cell was $\eta = 0.844 \pm 0.001$. The two cylinders were held concentric to within ± 0.003 cm by acrylic endcaps which also provide the fixed-end boundary conditions at the two axial extremes of the annulus. The aspect ratio, the ratio of the length of the annulus to the gap width, was $\Gamma = 37.5$.

The inner cylinder was driven by a stepper motor capable of microstepping at 25 000 steps per revolution producing a very smooth rotation. The rotational frequency of the inner cylinder was read by an optical encoder with a resolution of 300 pulses per revolution. A MacIntosh II with a MacADIOS data acquisition and control board oversaw the operation of both of these devices. The rotational speed of the inner cylinder was

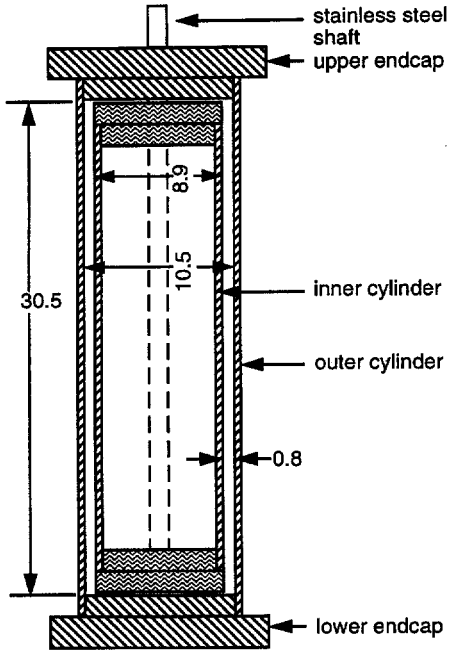

Fig. 1. Cross-sectional view of the experimental flow cell. All dimensions are in centimeters

controlled to better than 0.1% for the range of speeds used in these experiments.

The working fluid consisted of a mixture of water, glycerol, potassium thiocyanate (KSCN), and trace amounts of titanium dioxide particles (TiO_2). The potassium thiocyanate was used to increase the index of refraction of the fluid to match that of acrylic so that the laser beam was not refracted at the curved fluid-acrylic interface. The 0.2 μm titanium dioxide particles were added as LDV seed particles in a volume concentration of 2.0×10^{-4}%. Two different fluid mixtures were used, one with a kinematic viscosity of about 2 cSt and one with a kinematic viscosity of about 6 cSt.

One of the most difficult aspects of this work was ensuring adequate control of the viscosity of the working fluid because the viscosity of aqueous solutions of glycerol are very sensitive to temperature changes. Using a water jacket to control the temperature of the working fluid was impractical because it required the LDV receiving optics to be further from the flow and created more optical interfaces between the flow and the LDV, degrading signal quality. Instead, flush-mount thermistors were installed in the wall of the outer cylinder, so that the temperature of the working fluid could be continuously monitored. The temperature of the working fluid tracked the room temperature which varied by no more than $\pm 0.25\,^{\circ}C$ over the course of an experiment.

The uncertainty in the Reynolds number due to the variation in the inner cylinder speed, fluid viscosity, and other factors ranged from 1.9% to 2.8%. Estimating the uncertainties present in the measured velocity data was difficult. The systematic uncertainty in the velocity measurements resided primarily in two areas: the ability of seed particles to follow the flow and the fringe spacing in the measurement volume. The seed particles were assumed to follow the flow accurately because the Stokes

number for the working fluid flowing over a single particle was very much less than 0.14, the maximum Stokes number for which a particle will accurately follow that flow (Dring, 1982). The systematic uncertainty in the fringe spacing was estimated at 0.5%, based on the uncertainty in the intersection angle of the LDV beams. The resulting overall systematic uncertainty was 0.5%. The random uncertainty of the velocity measurements was more difficult to quantify. It was not possible to separate the random uncertainty associated with the measurements from the natural distribution of flow velocities within the measurement volume. Therefore, the standard deviation of the group of measurements taken at each measurement point constituted an estimate of the maximum random uncertainty, typically 2 to 3% of the inner cylinder speed.

For each Reynolds number at which velocity measurements were made, the annulus was filled with fluid, and the inner cylinder was run at high speed for a few minutes to thoroughly mix the fluid. Then the inner cylinder was stopped and the working fluid motion was allowed to decay to quiescence. Finally, the inner cylinder speed was ramped linearly to the desired speed. The slope of the linear ramp up to each Reynolds number was held constant at a relatively slow rate of 0.2 *Re*/sec for all Reynolds numbers at which measurements were made because of the sensitivity of the Taylor-Couette system to initial conditions. The dimensional ramp slope of 0.2 *Re*/sec corresponds to a dimensionless ramp slope $d(Re_C)/dt^*$ of about 80 for the 6 cSt fluid and about 240 for the 2 cSt fluid. Here we use the time scaling proposed by Park, et al. (1981), $t^* = t/(Ld/v)$, where L is the length of the annulus. After the inner cylinder reached the desired speed, the flow was allowed to develop at the Reynolds number for at least an hour to ensure that the flow was fully developed before measurements began. Consecutive measurements without changing the inner cylinder speed showed that the time allowed for the flow to develop was sufficient to generate repeatable results.

The flow velocities were measured using a TSI, Inc. laser Doppler velocimeter set up in an on-axis backscatter mode. A 5W Argon-Ion laser was used to generate the collimated coherent light for the LDV. The LDV measuring volume was a prolate ellipsoid of revolution with its major axis extending in the radial direction about 280 μm and a minor axis extending 80 μm. The measurement volume was positioned using a three axis traverse with a positioning accuracy of ±0.005 mm. A counter-type signal processor converted the bursts of light from particles passing through the measurement volume to velocity measurements. Typically, either 4 096 or 8 192 individual velocity measurements were collected at each measurement point. Collection of the individual velocity measurements took between 10 seconds and 1 minute per measurement point depending on the quality of the signal and the number of measurements collected.

4
Results and discussion

The azimuthal velocity profiles for the various flow regimes of interest were measured at a grid of evenly spaced points distributed in both the radial and axial directions. Typically ten measurement points were distributed radially across the annulus and about 35 to 45 were distributed axially, spanning a single pair of vortices. The azimuthal velocity measurements are normalized with respect to the azimuthal velocity of the inner cylinder. The position variable in the radial direction, $\xi = (r - r_i)/d$, is normalized with respect to the gap width so that it varies from $\xi = 0$ at the inner cylinder to $\xi = 1$ at the outer cylinder. The position variable in the axial direction, $\zeta = (z - z_0)/h$, is normalized with resepect to the vortex height h so that it varies from $\zeta = 0$ at the outflow region between a pair of vortices to $\zeta = \pm 1$ at the inflow region between neighboring pairs of vortices.

The azimuthal velocity profile was measured for the circular Couette flow regime to check the validity of the experimental procedure in a flow regime where a simple analytical solution exists. The azimuthal velocity was measured at a grid consisting of 11 points in the radial direction and 41 points in the axial direction. This grid of points was chosen to completely span the area of the flow cell that would be used in all subsequent measurements. The agreement between the experimental and analytical results was very good. These measurements were subsequently used to accurately determine the position of the inner and outer cylindrical boundaries with respect to the LDV traverse and to determine whether the axis of the flow cell was parallel to the axis of the LDV traverse.

4.1
Taylor vortex flow

The azimuthal velocity was measured at a large number of spatially-distributed points at a fixed Reynolds number to explore with high spatial resolution the radial and axial dependence of the velocity profile at a given Reynolds number. Because the measured azimuthal velocity is dependent on both the radial and axial position, the resulting velocity profiles are expressed as velocity contour plots in the $\xi - \zeta$ plane.

These contour plots of normalized azimuthal velocity, shown in Figs. 2a, 2b, represent the extremes of the Taylor vortex flow regime. Figure 2a shows a measurement made at a Reynolds

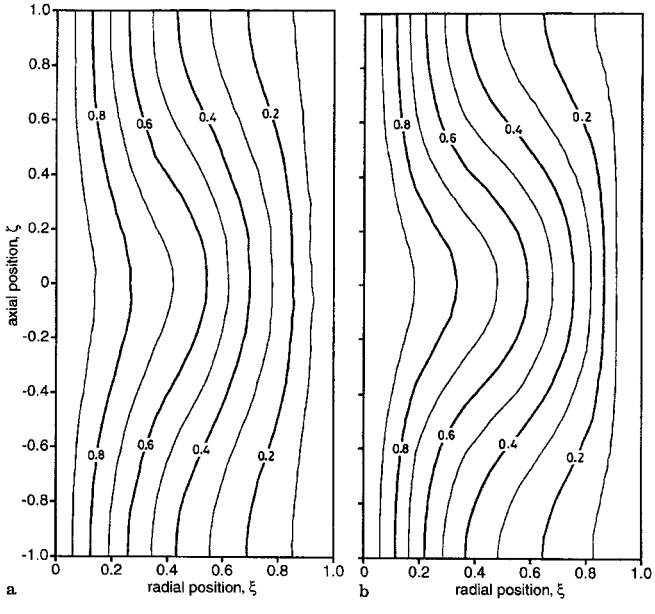

Fig. 2a, b. Contour plot of azimuthal velocity normalized with respect to the azimuthal velocity of the inner cylinder for the Taylor vortex flow regime for **a** $Re = 1.02\ Re_C$ and **b** $Re = 1.15\ Re_C$

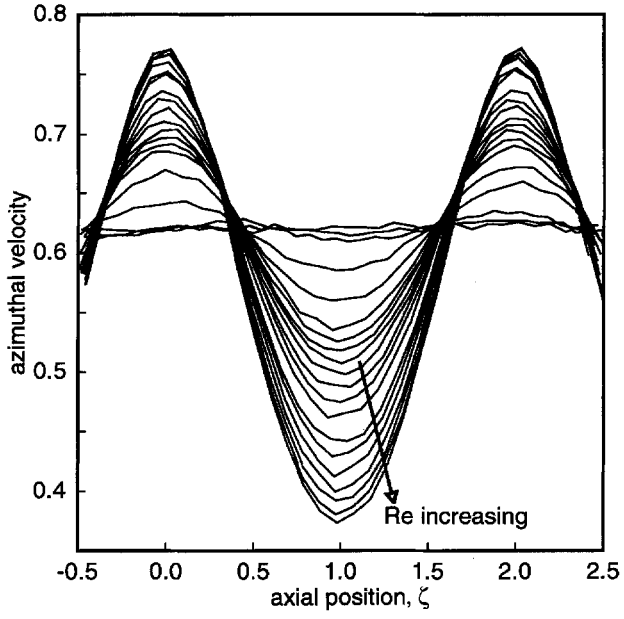

Fig. 3. Normalized azimuthal velocity measurements of the Taylor vortex flow regime at a series of Reynolds numbers for a fixed radial position ($\xi = 0.4$). The velocity decreases monotonically with increasing Reynolds number for $\zeta = 1$ and increases monotonically for $\zeta = 0$ and $\zeta = 2$

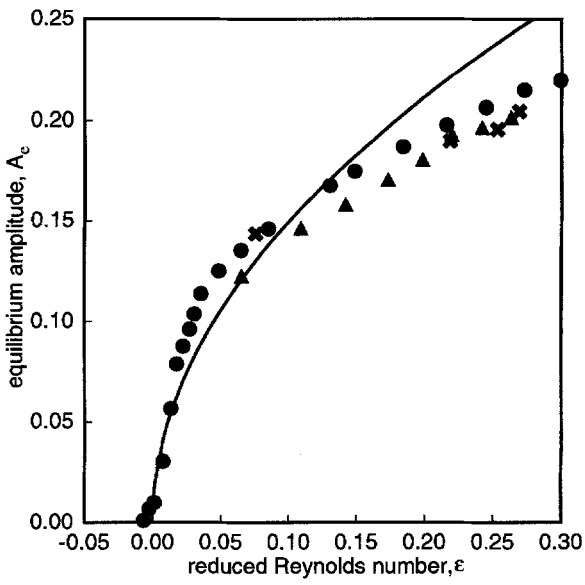

Fig. 4. Growth rate comparison of experimental and calculated equilibrium amplitudes A_e. The solid line represents Davey's 1962) calculation while the symbols represent three different experimental trials

number slightly greater than that required for the transition to Taylor vortex flow, $Re = 108 = 1.02\, Re_C$. Figure 2b shows a measurement made at a Reynolds number slightly less than that required for the transition to wavy vortex flow, $Re = 122 = 1.15 Re_C = 0.98 Re_C'$, where Re_C' is the Reynolds number at which the transition to wavy vortex flow occurs. The contours bulge outward in the radial outflow region at $\zeta = 0$ as high azimuthal momentum fluid is carried from near the inner cylinder outward by the secondary radial outflow. Similarly, the contours bulge radially inward in the inflow region at $\zeta = \pm 1$ where low momentum fluid from near the outer wall is carried inward by the secondary radial inflow. The contour lines in Fig. 2b are more sharply curved than those in Fig. 2a, indicating that the vortices strengthen wih increasing Reynolds number.

To determine the effect of Reynolds number on the velocity profile, the azimuthal velocity was measured at a few selected radial positions as a function of axial position for a series of Reynolds numbers. The number of distinct measurement points distributed in axial direction was the same as for the procedure used to obtain Figs. 2a and b. The results for a radial position near the center of the gap, $\xi = 0.4$, where the best LDV signal was attained, are shown in Fig. 3. Each curve in the Fig. 3 represents azimuthal velocity measurements for a different Reynolds number. The normalized azimuthal velocity increases monotonically with Reynolds number in the radial outflow region, $\zeta = 0$ and $\zeta = 2$, and decreases in the radial inflow region, $\zeta = 1$. Clearly, the axial average of the azimuthal velocity, normalized with respect to the inner cylinder speed, decreases as the Reynolds number increases. Since the radial position at which the measurements were made, $\xi = 0.4$, is closer to the inner cylinder than the outer cylinder, the decreasing velocity suggests steeper radial gradients of the azimuthal velocity near the inner cylinder. In addition, the amplitude of the waveform increases with increasing Reynolds number, suggesting stronger Taylor vortices.

The Davey (1962) solution for the velocity profile in the Taylor vortex flow regime was computed to second order accuracy in $A_e(\varepsilon)$ for the radius ratio $\eta = 0.844$ to match the experimental conditions. Then the Davey solution was fit to each set of experimental velocity measurements made at a particular Reynolds number by iteratively adjusting the equilibrium amplitude A_e, the critical Reynolds number Re_C, and the fundamental wavenumber of the disturbance λ until the least squares difference between the two velocity fields was minimized. The least squares difference Δ_{ls} between the experimental velocity field and the second order accurate Davey expansion is given by

$$\Delta_{ls} = \sum_{r,z} [v_\theta(r, z, \varepsilon)_{\exp} - v_\theta(r, z, \varepsilon)_{\text{Davey}}]^2$$

$$= \sum_{r,z} [v_\theta(r, z, \varepsilon)_{\exp} - \bar{v}_c(r) - A_e(\varepsilon) v_{10}(r) \cos \lambda z$$

$$- A_e(\varepsilon)^2 \{f_1(r) + v_{20}(r) \cos 2\lambda z\}]^2 \qquad (7)$$

The equilibrium amplitudes calculated from the Δ_{ls} procedure are compared to Davey's predicted growth rate of A_e, given in Eq. (6), as a function of reduced Reynolds number ε in Fig. 4. This figure differs significantly from those in previous works (Berland et al., 1986; Gollub and Freilich, 1976; Heinrichs et al., 1988; Snyder and Lambert, 1966) in that it is a plot of equilibrium amplitude A_e, not the relative amplitude of the individual Fourier coefficients. The critical Reynolds number Re_C for the experimental data was determined by iteratively adjusting Re_C until the least squares difference between the experimental data and Davey's predicted curve was minimized. The critical Reynolds number for the experimental data was found to be somewhat smaller (about 2%) than the value calculated using the Davey expansion. Berland, et al. (1986) also found a critical

Reynolds number somewhat lower than that calculated by linear stability. The experimentally determined A_e grows approximately as $\sqrt{\varepsilon}$, as Davey predicted, for small ε. For $\varepsilon > 0.15$, A_e grows somewhat more slowly than predicted.

One possible explanation for the difference between the predicted and experimental growth rates is that the expansion parameter ε has exceeded the range of validity of the second order Davey expansion, $\varepsilon \ll 1$. The range of validity of the expansion could be extended by increasing the order of the expansion. Although Snyder and Lambert (1966) found reasonable agreement between a second order expansion and experimental results, Edwards, et al. (1991) and Raffai and Laure (1993) found a discrepancy similar to that in Fig. 4 between a third order expansion and fully nonlinear numerical results, indicating that increasing the order of the expansion may produce better agreement between experimental and analytical results. Another possible explanation for the difference is that the speed of the inner cylinder may have been ramped too quickly from rest to the speed at which the measurements were made. The procedure used in these experiments was shown to generate self-consistent, repeatable results using a ramp rate of $d(Re)/dt^* \approx 80$. Nevertheless, Park, et al. (1981) reported that a dimensionless ramp rate of $d(Re)/dt^* \leqslant 20$ was necessary to eliminate hysteresis in the development of Taylor vortices. The deviation of the experimentally calculated growth rate from Davey's prediction may be related to this hysteresis. The parameter k from Eq. (6) was found for the experimental data by the same best fit procedure used to find Re_C. The value of k from the Davey expansion, $k = 4.55 \times 10^{-3}$, compares well with that for the experimental data, $k = 4.13 \times 10^{-3}$.

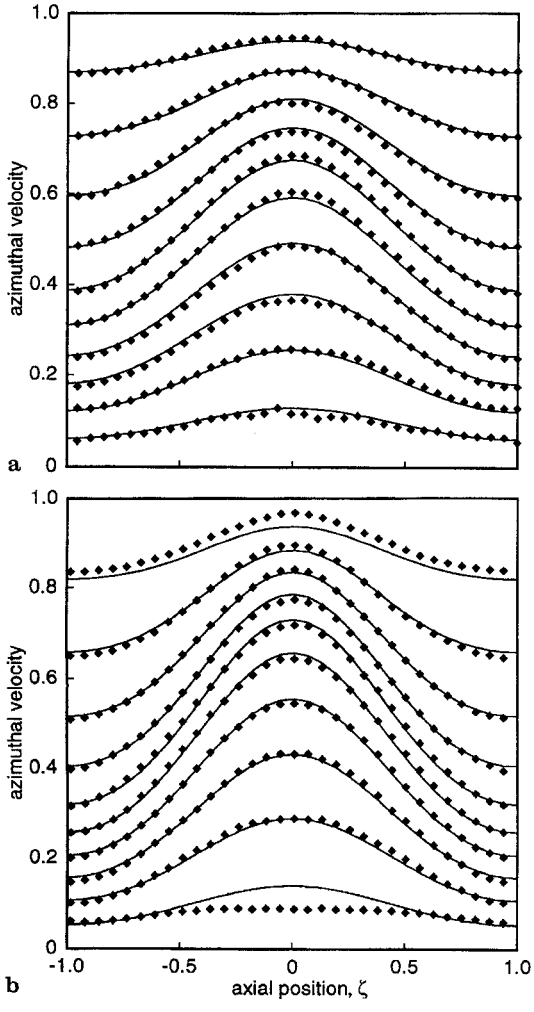

Fig. 5a, b. Comparison of calculated and experimental azimuthal velocity fields in the Taylor vortex flow regime for **a** $Re = 1.02\ Re_C$ ($\varepsilon = 0.04$) and **b** $Re = 1.15\ Re_C$ ($\varepsilon = 0.25$). The curves represent Davey's (1962) calculations while the symbols represent experimental measurements. The data are grouped by radial position. The radial positions for **a** are evenly spaced between $\zeta = 0.104$ (bottom) and $\zeta = 0.930$ (top), while for **b** they are evenly spaced between $\zeta = 0.091$ (bottom) and $\zeta = 0.909$ (top)

A comparison between the experimental and calculated azimuthal velocity fields is shown in Figs. 5a and b for the two Reynolds numbers at the extremes of the Taylor vortex flow regime shown in Figs. 2a and b. Figures 5a and b show azimuthal velocity measurements made at a grid of radial and axial points. Each curve represents measurements made at the same radial position, with the curves at lower azimuthal velocities for radial positions closer to the outer cylinder. The Davey solution agrees quite well with the experimental data. The RMS difference between the two velocity fields is 0.59% of the inner cylinder speed for the lower Reynolds number, $Re = 108$, and 1.15% for the higher Reynolds number, $Re = 122$. The uncertainty in the azimuthal velocity measurements, averaged over the entire velocity field, is 3.0% of the inner cylinder speed for Fig. 5a and 2.6% for Fig. 5b. In other words, the RMS difference between the Davey expansion and the measured velocity field much smaller than the scatter in the velocity measurements. The correlation between theory and experiment is better at the lower Reynolds number, since Davey's expansion is most valid there. The deviation between theory and experiment at the higher Reynolds number is most evident for the curves representing the velocity near the walls, perhaps due to the difficulty associated with making LDV measurements near the walls.

4.2
Wavy vortex flow

Wavy vortex flow consists of toroidal vortices with an azimuthally traveling waviness superimposed on the vortices (Andereck et al., 1986). The high spatial resolution velocity measurement procedure from the previous section was used for the wavy vortex flow regime with slight modifications. The azimuthally traveling waves cause the velocity measured at a fixed point to be time-dependent. Since it is difficult to measure a time dependent full-field velocity profile with a single measurement point LDV, the velocity at each measurement point was averaged in time yielding a time-averaged, full-field velocity profile. Averaging out the time dependence of the velocity profile required collecting a larger number of individual velocity measurements than in the time independent case to generate a stationary mean velocity. In general, the duration of the velocity measurement at each measurement point was long enough to let at least ten traveling waves pass.

Figures 6a–d shows the development of the time-averaged velocity contours with increasing Reynolds number, from $Re = 1.18\ Re_C = 1.01\ Re_C'$ to $Re = 12.45\ Re_C$. Just above the transition to wavy vortex flow the velocity contour plot, Fig. 6a, is similar to the Taylor vortex flow plot shown in

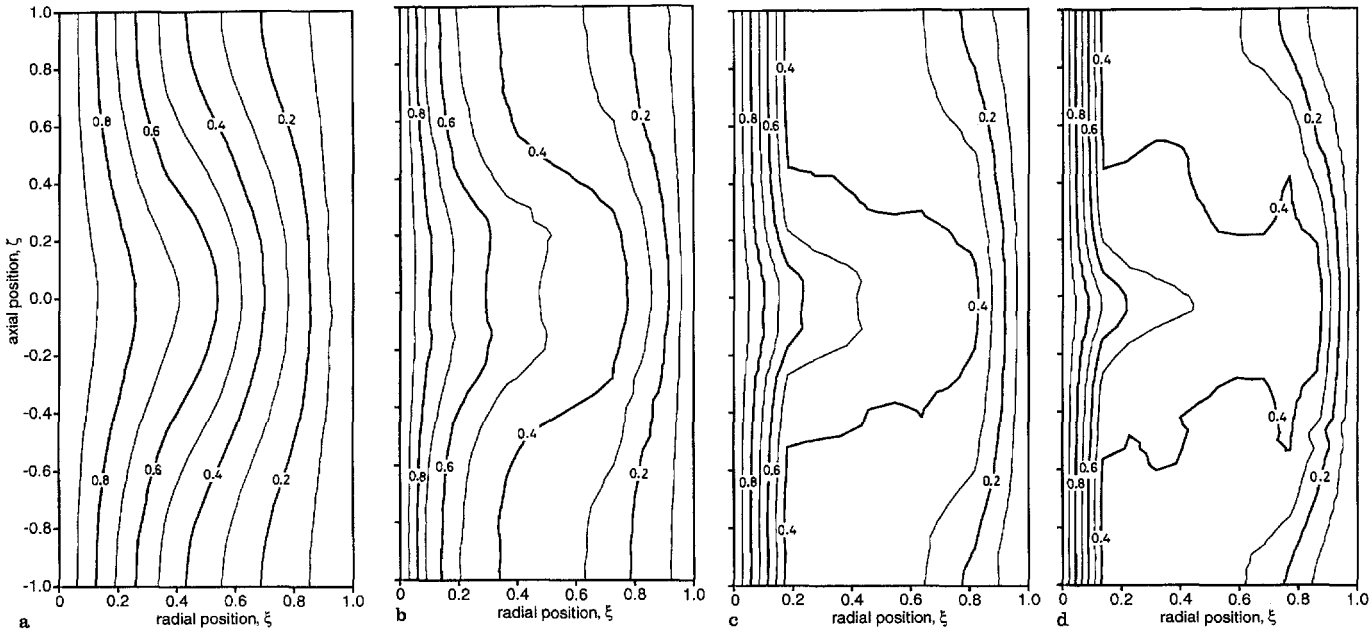

Fig. 6a–d. Contour plot of normalized azimuthal velocity for the wavy vortex flow regime for **a** $Re = 1.18\, Re_C$, **b** $Re = 3.23\, Re_C$, **c** $Re = 8.18\, Re_C$, and **d** $Re = 12.45\, Re_C$

Fig. 2b. The contours are slightly more sharply curved, indicating a marginally stronger vortex flow at the higher Reynolds number. Between Figs. 6a and b, the velocity contours change significantly as the Reynolds number increases from $1.18\, Re_C$ to $3.23\, Re_C$. The contours become flattened in the both the radial outflow and inflow regions. The radial outflow region has a smaller axial extent than the radial inflow region. In addition, the azimuthal velocity gradients at the inner and outer walls are steeper at the higher Reynolds number. As the Reynolds number is increased to $8.18\, Re_C$, in Fig. 6c, the velocity gradients at the inner and outer walls become even steeper. In addition, the radial outflow region becomes still narrower, suggesting a jet-like radial outflow.

Figure 6d is a contour plot of azimuthal velocity measurements made at $Re \approx 12.45\, Re_C$, corresponding to modulated wavy vortex flow (Andereck et al., 1986). The velocity gradients at the inner and outer cylinder have steepened further. At this Reynolds number adverse velocity gradients appear. At the axial position $\zeta = \pm 0.4$, the azimuthal velocity no longer monotonically decreases from the inner cylinder to the outer cylinder. Near the middle of the gap, between $\xi = 0.4$ and $\xi = 0.8$, there is a region in which the azimuthal velocity decreases, increases, then decreases again with increasing radial position. Coughlin and Marcus (1992) found similar adverse velocity gradients for $\eta = 0.875$ and $\mathrm{Re} = 8\, Re_C$ (also modulated wavy vortex flow) using a pseudospectral initial-value code to study the nonlinear development of Taylor vortices. Apparently the outflow jet is so strong that high azimuthal momentum fluid carried outward by the jet encounters the outer wall where it must turn and proceed axially, creating the adverse velocity gradient.

4.3
Turbulent Taylor vortex flow

The azimuthal velocity in the turbulent Taylor vortex flow regime was difficult to measure because a large number (40 960) of individual velocity measurements had to be made at each measurement point to assure that the mean of the individual measurements was stationary. Collecting 40 960 individual velocity measurements at each measurement point required several minutes per measurement point. In order that the overall experiment time not be prohibitively long, the number of spatial points at which velocity measurements were made was reduced so that the overall experiment time was the same as for the preceding flow regimes, about four to six hours. The grid of measurement points for the turbulent Taylor vortex flow regime consisted of a grid of 4 evenly spaced points in the radial direction and about 40 in the axial direction.

Figure 7 shows the velocity contours for the turbulent Taylor vortex velocity measurements at a Reynolds number of $\mathrm{Re} \approx 9\,800 \approx 92 Re_C$. At this high Reynolds number, the turbulent mixing and fluid transport by the vortices have very effectively mixed the fluid in the middle portion of the annulus gap, between $\xi = 0.2$ and $\xi = 0.8$. There remains signs of the radial outflow and inflow regions at $\zeta = 0$ and ± 1, respectively. There is also evidence of high momentum fluid from near the inner cylinder being carried outward and then back inward by the vortices in the center of the gap as illustrated by the dashed contour in Fig. 7. Since the spatial resolution of the measurement points in the radial direction is reduced from that in the previous plots, the velocity gradients near the inner and outer cylindrical boundaries do not appear to be as steep as they actually are. With sufficient spatial resolution, the velocity gradients near the boundaries would be very steep and the region between these boundary layers would have a nearly uniform azimuthal velocity.

4.4
Dependence of velocity profile on Reynolds number

Several numerical simulations of the wavy vortex flow regime have been reported (Coughlin and Marcus, 1992; Marcus, 1984;

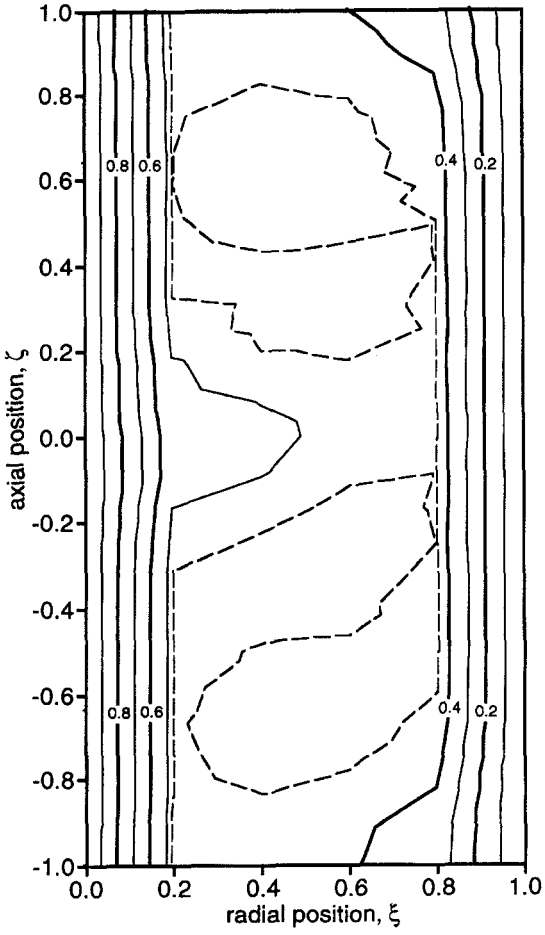

Fig. 7. Contour plot of azimuthal velocity for the turbulent Taylor vortex flow regime for $Re \approx 92\, Re_C$. The dashed contour, corresponding to a normalized azimuthal velocity of 0.47, reveals the transport of high momentum fluid by the vortex

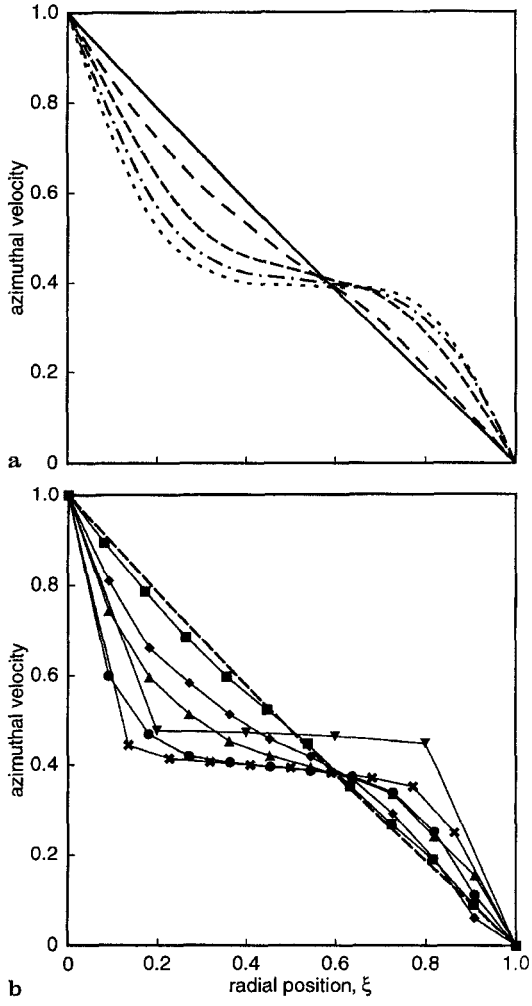

Fig. 8a, b. Comparison of numerical and experimental axially-averaged azimuthal velocity data. The numerical results of Marcus (1984) in a are for circular Couette flow (solid), $Re = 1.18\, Re_C$ (long dashed), $Re = 2.06\, Re_C$ (medium dashed), $Re = 2.95\, Re_C$ (dot-dashed), $Re = 3.96\, Re_C$ (short dashed). Experimental measurements are shown in b for $Re = 1.02\, Re_C$ (■), $Re = 1.70\, Re_C$ (◆), $Re = 3.23\, Re_C$ (▲), $Re = 4.81\, Re_C$ (●), $Re = 12.45\, Re_C$ (×), $Re = 92\, Re_C$ (▼). The dashed curve is the analytic solution for circular Couette flow

Moser et al., 1983) although the one by Marcus (1984) is the most useful for comparison to our experimental results. He used a pseudospectral code to calculate axially-averaged angular momentum profiles for a series of Reynolds numbers distributed throughout both the Taylor vortex and wavy vortex flow regimes. Marcus' results for a radius ratio $\eta = 0.875$ are replotted in Fig. 8a as axially-averaged azimuthal velocity profiles. Marcus' data tends toward a velocity profile that is flat throughout the center portion of the gap, and increasingly steep near the boundaries as the Reynolds number increases. The same trend is evident in the experimental axially-averaged azimuthal velocity profiles for the Taylor vortex and wavy vortex flow regimes shown in Fig. 8b. Both sets of data tend toward the same normalized azimuthal velocity in the center of the gap, about 40% of the inner cylinder speed. The turbulent velocity profile for $Re \approx 92\, Re_C$ is also shown in Fig. 8b. It has a noticeably higher velocity in the center of the gap, about 45% of the inner cylinder speed, probably as a result of turbulent mixing in addition to transport by the vortices.

5
Conclusions

Our first goal in this work was to verify the analytical prediction made by Davey (1962) for Taylor vortex flow by comparing it to the experimentally measured azimuthal velocity field. Previous experimental work has shown that the amplitude of individual Fourier coefficients of the disturbed velocity field increase with Reynolds number (Berland et al., 1986; Gollub and Freilich, 1976; Heinrichs et al., 1988; Snyder and Lambert, 1966) suggesting that the strength of vortices for Taylor vortex flow increases as predicted by Davey. Nevertheless, the growth of the equilibrium amplitude A_e with Reynolds number has not been addressed experimentally. Here we have found that for small ε, the equilibrium amplitude A_e indeed grows nearly as Davey predicted, as shown in Fig. 4. While these results are not surprising, they are the first full experimental confirmation of the validity of Davey's analysis.

What is surprising, though, is how well the experimental results compare with Davey's expansion of the velocity field, especially at higher ε. Davey provided expressions for the velocity field in Taylor vortex flow for two particular radius

ratios. Nevertheless, the researchers who subsequently examined the validity of the perturbation expansion did not rework the solution at the radius ratio at which their experimental results were obtained, nor did they compare the full analytical velocity field to their experimental results. Here we used the experimentally determined equilibrium amplitude A_e in Eqs. (1)–(3) to analytically calculate the azimuthal velocity field based on Davey's perturbation expansion. Not only does the analytically determined velocity field match the experimental data for small ε as shown in Fig. 5a, it matches quite well for ε as large as 0.28 as shown in Fig. 5b, except very near the walls of the annulus. Even if Davey's theoretical equilibrium amplitude, shown in Fig. 4, is used to obtain the analytical velocity field, the agreement between the analytical prediction and the experimental velocity field is quite good. In addition, Fig. 5 confirms the radial dependence of Davey's expansion, especially near $\varepsilon = 0$ where the expansion is most accurate.

Our second goal in this research was to determine the effect of the Reynolds number on the strength of vortices and the structure of the azimuthal velocity field for several different flow regimes of supercritical circular Couette flow. These results were presented as azimuthal velocity contours for different Reynolds numbers, shown in Figs. 2, 6, and 7. The vortices carry high azimuthal momentum fluid from near the inner wall outward at outflow regions between vortices and carry low azimuthal momentum fluid from near the outer wall inward at inflow regions. For Taylor vortex flow this results in a waviness of the azimuthal velocity contours. As the Reynolds number increases, the contours become more sharply curved because of the stronger vortices. As the Reynolds number is increased to wavy and modulated wavy vortex flow, the radial transport of azimuthal momentum fluid away from the walls increases as the vortices increase in strength. This results in a nearly uniform azimuthal velocity across a broad portion of the annular gap with steep, boundary layer-like velocity gradients near the walls of the annulus confirming the numerical simulation of wavy vortex flow (Marcus, 1984). As the Reynolds number increases, the outflow regions become jet-like, although the inflow regions, while increasing in strength, are weaker. Finally, as the Reynolds number is increased to turbulent vortex flow, the turbulent mixing and fluid transport by the vortices mixes the fluid in the middle portion of the annular gap resulting in a region of nearly uniform azimuthal velocity with steep boundary layers near the walls. For turbulent vortex flow, the outflow can be so strong that high azimuthal momentum fluid is carried radially outward and then axially, resulting in adverse radial velocity gradients.

References

Andereck CD; Liu SS; Swinney HL (1986) Flow regimes in a circular Couette system with independently rotating cylinders. J Fluid Mech 164: 155–183

Berland T; Jøssang T; Feder J (1986) An experimental study of the connection between the hydrodynamic and phase-transition descriptions of the Couette-Taylor instability. Phys Scipta 34: 427–431

Chandrasekhar S (1958) The stability of viscous flow between rotating cylinders. Proc Roy Soc London A 246: 301–311

Coughlin KT; Marcus PS (1992) Modulated waves in Taylor-Couette flow. Part 2. Numerical simulation. J Fluid Mech 234: 19–46

Davey A (1962) The growth of Taylor vortices in flow between rotating cylinders. J Fluid Mech 14: 336–368

Donnelly RJ; Simon NJ (1960) An empirical torque relation for supercritical flow between rotating cylinders. J Fluid Mech 7: 401–418

Dring RP (1982) Sizing criteria for laser anemometry particles. ASME J Fluid Eng 104: 15

Edwards WS; Tagg RP; Dornblaser BC; Swinney, HL (1991) Periodic traveling waves with nonperiodic pressure. Eur J Mech, B/Fluids 10(2-Suppl.), 205–210

Gollub JP; Freilich MH (1976) Optical heterodyne test of perturbation expansions for the Taylor instability. Phys Fluids 19: 618–626

Gollub JP; Swinney HL (1975) Onset of turbulence in a rotating fluid. Phys Rev Lett 35: 927–930

Heinrichs RM; Cannell DS; Ahlers G; Jefferson M (1988) Experimental test of the perturbation expansion for the Taylor instability at various wavenumbers. Phys Fluids 31: 250–255

Mallock A (1888): Determination of the viscosity of water. Proc Roy Soc London A 45: 126–132

Marcus PS (1984) Simulation of Taylor-Couette flow. Part 2. Numerical results for wavy-vortex flow with one travelling wave. J Fluid Mech 146: 65–113

Moser RD; Moin P; Leonard A (1983) A spectral numerical method for the Navier Stokes equations with applications to Taylor-Couette flow. J Comp Phys 52: 524–544

Park K; Crawford GL; Donnelly RJ (1981) Determination of transition in Couette flow in finite geometries. Phys Rev Lett 47: 1448–1450

Raffai R and Laure P (1993) Influence of an axial mean flow on the Couette-Taylor problem. Eur J Mech B/Fluids 12: 277–288

Smith GP; Townsend AA (1982) Turbulent Couette flow between concentric cylinders at large Taylor numbers. J Fluid Mech 123: 187–217

Snyder HA; Lambert RB (1966) Harmonic generation in Taylor vortices between rotating cylinders. J Fluid Mech 26: 545–562

Stuart JT (1960) On the non-linear mechanics of wave disturbances in stable and unstable parallel flows. Part 1. The basic behaviour in plane Poiseuille flow. J Fluid Mech 9: 353–370

Taylor GI (1935) Distribution of velocity and temperature between concentric rotating cylinders. Proc Roy Soc A 151: 494–512

Taylor GI (1923) Stability of a viscous liquid contained between two rotating cylinders. Phil Trans A 223: 289–343

Watson J (1960) On the non-linear mechanics of wave distrubances in stable and unstable parallel flows. Part 2. The development of a solution for plane Poiseuille flow and for plane Couette flow. J Fluid Mech 9: 371–389